On integration of rock physics in quantitative seismic interpretation

Kenneth Bredesen

Dissertation for the degree of philosophiae doctor (PhD)

at the University of Bergen

2016

Preface

This thesis is submitted for fulfillment of the degree of Philosophiae Doctor (PhD) at the Department of Earth Science at University of Bergen. Financial support were given by Tullow Oil, Christian Michelsen Research and Statoil. The motivation for this PhD project was to extend research on the *Inverse Rock Physics Modeling* methodology which I used in my thesis for obtaining the Master of Science degree at the Department of Earth Science at University of Bergen.

The work presented in this thesis was initiated during summer 2012 with a three year PhD contract with the University of Bergen. The main work was conducted in Bergen with some occasional visits to Tullow Oil in Oslo for supervision. The thesis is based on one conference paper and four research papers published or submitted to peer-reviewed scientific journals.

My principal supervisor for this study was Professor Tor Arne Johansen at the University of Bergen and my co-supervisors were Dr. Erling Hugo Jensen at Rock Physics Technology and Dr. Per Avseth at Tullow Oil.

The thesis is organised as follows. The overall study objectives are given prior to a general introduction which gives a short review of some basic terminology and relevant background theory used throughout this study. Then, the main scientific contributions of the papers are summarized before the overall conclusions of the thesis are presented. Finally, the papers in full forms can be found in the appendix.

Kenneth Bredesen

Kenneth Bredesen
Bergen, November 3, 2016

Acknowledgements

I would like to thank those whom I couldn't be without to fulfill this thesis. First of, I feel privileged to be surrounded by a great team of supervisors: Tor Arne Johansen, Erling Hugo Jensen and Per Avseth. Thanks for letting me take part in such exciting research and for the scientific and moral support along the way. Our regular meetings have been filled with interesting discussions and constructive feedback which have been essential for my progress. A special thank goes to Erling for sharing his office with me and making guidance easy available.

Attending various conferences and courses in all from Henningsvær in Lofoten to Houston in Texas have been inspiring both on a scientific and social level. In particular, I will never forget my two months stay at the University Centre in Svalbard... shooting seismic on top of fjord ice, driving snowmobiles over glaciers and scouting for polar bears in a majestic scenery; a priceless experience.

Thanks to my fellow students for being good friends and adding joy to both in and outside University campus. I have great memories from our enthusiastic lunch discussions, gym workouts, mountain hiking, taco Fridays, etcetera. Our companionship is very much appreciated and I am looking forward to stay in touch.

My family have always encouraged and motivated me on my journey through higher education. Thanks for making me feel welcome back home anytime and for always believing in me, it means a lot.

And finally, there is my girlfriend Rikke who lights up my everyday by just being her own positive and social being. Thank you for your support and showing that you are proud of me. I am lucky to have you in my life.

List of papers

Conference paper Bredesen K., Jensen E.H. and Johansen T.A. 2013. Inverse Rock Physics Modelling on Spatially Varying Seismic Parameters. Conference paper, presented at the 75^{th} *EAGE Conference & Exhibition*, London, 10-13 June.

Paper 1 Bredesen K., Jensen E.H., Johansen T.A. and Avseth P. 2015. Quantitative seismic interpretation using inverse rock physics modeling. *Petroleum Geoscience*, vol. 21, no. 4, 271-284.

Paper 2 Bredesen K., Jensen E.H., Johansen T.A. and Avseth P. 2015. Seismic reservoir and source-rock analysis using inverse rock-physics modeling: A Norwegian Sea demonstration. *The Leading Edge*, vol. 34, no. 11, 1350-1355.

Paper 3 Jensen E.H., Johansen T.A., Avseth P. and Bredesen, K. 2016. Quantitative interpretation using inverse rock-physics modeling on AVO data. *The Leading Edge*, vol. 35, no. 8, 677-683.

Paper 4 Bredesen K., Avseth P., Johansen T.A. and Olstad R. 2016. Rock physics modelling based on depositional and burial history of Barents Sea sandstones. Submitted to *Petroleum Geoscience*.

Authorship statement

The authors contributions to each paper are specified as follows:

Conference paper

Text and figures	Bredesen
Method programming	Johansen, Jensen
Application programming and modeling	Bredesen
Manuscript discussion and review	Bredesen, Jensen, Johansen

Paper 1

Text and figures	Bredesen
Method programming	Johansen, Jensen
Application programming and modeling	Bredesen
Manuscript discussion and review	Bredesen, Jensen, Johansen, Avseth

Paper 2

Text and figures	Bredesen
Method programming	Johansen, Jensen
Application programming and modeling	Bredesen, Jensen
Manuscript discussion and review	Bredesen, Jensen, Johansen, Avseth

Paper 3

Text	Jensen
Figures	Jensen, Bredesen
Method programming	Johansen, Jensen
Application programming and modeling	Jensen, Bredesen
Manuscript discussion and review	Jensen, Johansen, Avseth, Bredesen

Paper 4

Text	Bredesen, Avseth, Olstad
Figures	Bredesen
Method programming and modeling	Bredesen
Basin modeling	Olstad
Manuscript discussion and review	Bredesen, Avseth, Johansen

Table of Contents

"To avoid situations in which you might make mistakes may be the biggest mistake of all."

Peter McWilliams

American author (1949-2000)

1 Objectives

The main objectives of this research have been to study methods for quantitative seismic interpretation which are consistent with rock physics and geological foundation. This has been achieved by:

- Extending areas of application and performing feasibility studies applying inverse rock physics modeling to seismic data.
- Performing rock physics modeling conditioned by burial history of uplifted Barents Sea sandstones.

Synthetic and real data from the Norwegian continental shelf is used to demonstrate performance and field applications of our geophysical analysis.

"You can't always get what you want,
but if you try sometimes,
you just might find,
what you need."

In "You can't always get what you want"
by **The Rolling Stones**

English rock band (1962)

2
Introduction

Much of the undiscovered hydrocarbons hides within smaller, more complex and deeper reservoirs requiring new and sophisticated methods for successful exploration and reservoir characterization. For this task we want quantities of reservoir parameters such as porosity, rock type and fluid saturation. However, what is actually acquired during field operations are typically quantities derived from well logs and seismic data which are all indirectly related to various reservoir parameters. Seismic observables are frequency bandlimited reflection signals which can be used to derive properties such as P- and S-wave velocities and acoustic impedances of the various layers. Going further, integrating rock physics with seismic data, well data and geological information opens up for direct predictions of reservoir parameters for better quantitative seismic interpretations (QSI). Figure 2.1 shows the concepts of such an integrated seismic-to-reservoir

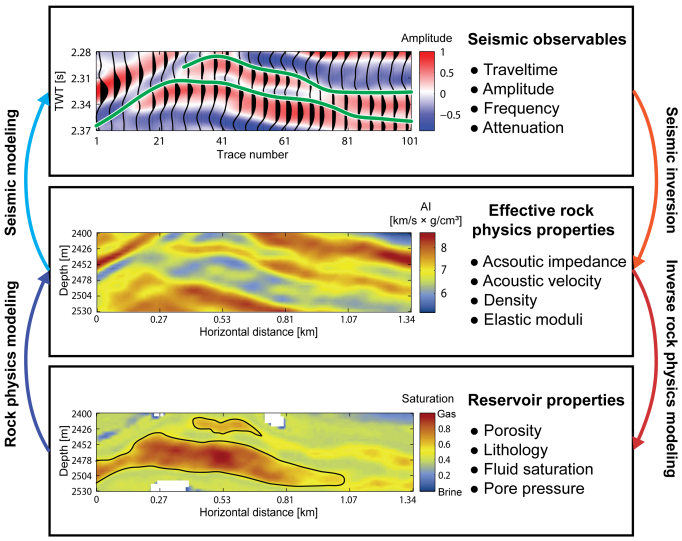

Figure 2.1: The links between acquired seismic data and desired reservoir properties. The illustration is from results in Paper 1 based on Norwegian Sea data and shows examples of parameters in each step.

workflow to better access quantitative reservoir parameters than possessed in conventional interpretation. However, due to natural variabilities in rock composition, constituent properties and textural complexities, a wide range of rock physics models have been developed, each one applicable to certain rock types. These models reveal that different rock types can exhibit similar seismic properties and associated seismic responses.

An example is misinterpreting organic source rocks as hydrocarbon saturated reservoir sandstones (Avseth and Carcione 2015). In Figure 2.2 we illustrate this by using rock physics templates (Ødegaard and Avseth 2004), where model trends are used to interpret data (see section 2.6.3 for more details). The two different rock types exhibit overlapping seismic properties which reduce our ability to differentiate them. This is an example taken from Paper 2 where models are locally calibrated, but other models might yield different results. In particular, source rocks are very difficult to model due to complex pore geometries, varying organic content and maturation; leading to large variations of possible seismic responses.

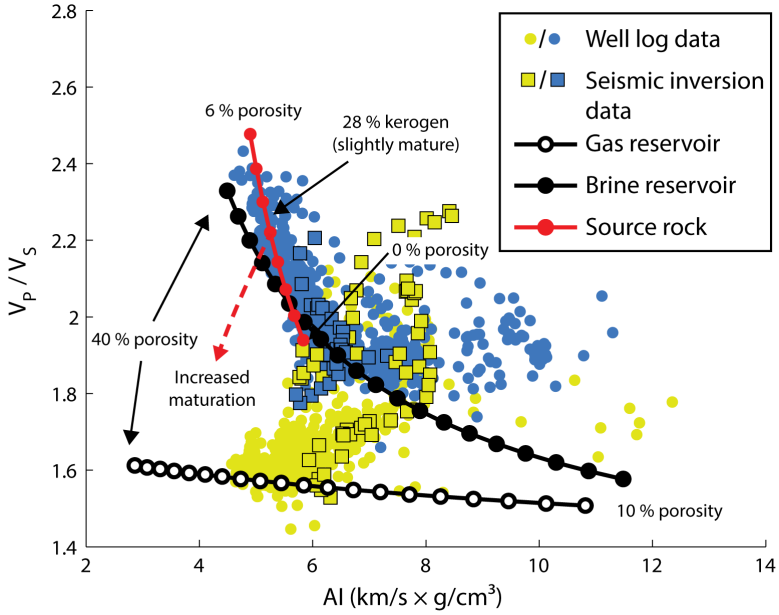

Figure 2.2: Cross-plot of Norwegian Sea seismic inversion data (square symbols) and well log data (dot symbols) superimposed by templates of rock physics models for slightly mature source rocks and gas and brine saturated sandstones. Data representing source rocks and gas saturated reservoir sandstones are plotted in blue and yellow, respectively. Increased maturation and hydrocarbon expulsion imply decreasing AI and V_p/V_s (Qin et al. 2014), as illustrated by the red arrow.

Another challenge which contributes to non-unique predictions, is that we have fewer different types of observables compared to the number of different reservoir properties which we want to estimate, i.e. the problem is underdetermined. This study therefore aims to further strengthen

rock physics consistent applications in a QSI workflow where the non-uniqueness of the problem is addressed and all possible solutions can be analyzed. Following is a brief introduction to some basic terminology and background theory relevant for this study.

2.1 Formation of hydrocarbon reservoirs

Sedimentary rocks are the main lithology for storage of hydrocarbons. Sediments are formed as minerals are eroded from the Earth's surface, subsequently transported and deposited to form a sedimentary basin. Through millions of years of deposition, the sediment compacts and consolidates, i.e. from loose granular aggregates to stiff rocks as temperature and pressure increase with depth. Also, large amounts of organic matter from dead plants and animals are periodically deposited and preserved within the sediments. Organic matter will transform into a solid material called kerogen that, eventually, fluidize into hydrocarbons and leaves its source rock migrating towards the surface. If trapped by a non-permeable cap rock, the hydrocarbons can accumulate within a porous reservoir rock.

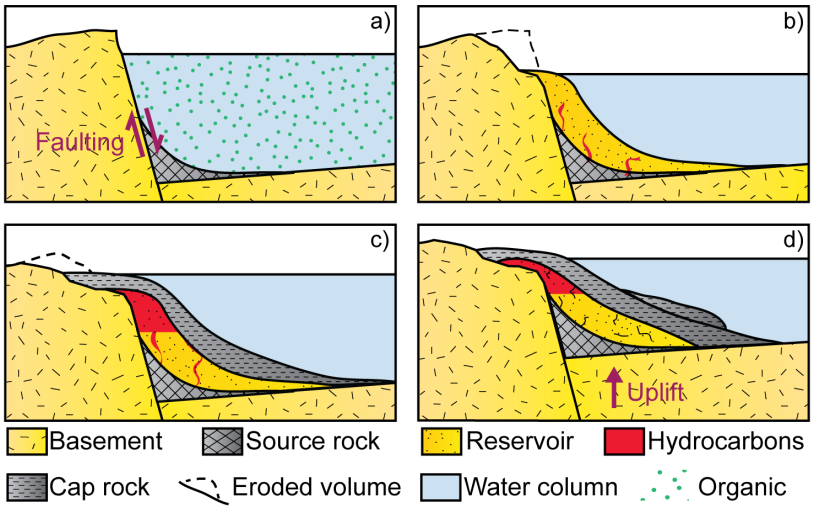

Figure 2.3: The evolution of a sedimentary basin forming a hydrocarbon reservoir with subsequent uplift events.

Figure 2.3 shows a simplified model for the evolution of a siliciclastic reservoir which has subsequently been uplifted: (a) organic matter is mixed with sediments forming a source rock, (b) shallow water sediments are deposited and subsequently infiltrated by hydrocarbons migrated from the source rock, (c) deep water deposits forms a non-permeable cap-rock such that hydrocarbons accumulate in the reservoir, and (d) tectonic forces yields uplift events such that overburden rocks are exposed to erosion.

2.2 Reservoir properties

In reservoir characterization various parameters are used to describe the rock qualities and properties. In the following, some of the relevant parameters for this study are defined.

Rocks are composites of solids and pores which fluids may occupy. The volume fraction of the pores relative to the total volume of rock is called porosity and is defined as

$$\phi = \frac{V_{pore}}{V_{solid} + V_{pore}}, \tag{2.1}$$

where V_{pore} and V_{solid} are the total volumes of pores and solids of the rock, respectively. Knowing the porosity is essential for estimating the potential hydrocarbon volumes within a reservoir.

The pores can contain mixtures of water, oil and gas. Fluid saturation S_m denotes the relative volume fraction of the porosity occupied by a fluid identified by index m. In case of M pore fluids, we have

$$\sum_{m=1}^{M} S_m = 1. \tag{2.2}$$

The mineral composition of the solid rock defines the type of lithology. The volume fraction V_n of a mineral type identified by index n, denotes the volume fraction for that mineral of the solid part of the rock, i.e. $(1 - \phi)$. For N types of minerals, we have

$$\sum_{n=1}^{N} V_n = 1. \tag{2.3}$$

For siliciclastic reservoirs, a binary mineral composition of clay and quartz is often considered. Then we often use the lithology parameter C, which is equal to the volume fraction of clay of the solid part of the rock.

2.3 Effective rock physics properties

The effective rock physics properties depend on the rock composition and the physical properties and geometrical distributions of constituents. Hence, the parameters described in the previous section have a direct impact on the effective rock physics properties. This link is described by rock physics equations which are discussed later in section 2.5. Below is a brief review of some basic rock physics properties used throughout this research; for more details see Mavko et al. (2009).

The velocities of pressure (or compressional) waves (V_p) and shear waves (V_s) propagating

through elastically isotropic rocks are given by

$$V_p = \sqrt{\frac{K + {}^4\!/_3\mu}{\rho}}, \tag{2.4a}$$

$$V_s = \sqrt{\frac{\mu}{\rho}}, \tag{2.4b}$$

where K and μ are the bulk and shear moduli expressing a rock's ability to resist changes in volume and shape, respectively. Accordingly, we have

$$\mu = V_s^2 \rho, \tag{2.5a}$$

$$K = \rho \left(V_p^2 - \frac{4}{3} V_s^2 \right), \tag{2.5b}$$

where the effective density ρ is given by

$$\rho = (1 - \phi) \sum_{n=1}^{N} V_n \rho_n + \phi \sum_{m=1}^{M} S_m \rho_m, \tag{2.6}$$

where ϕ, V_n and ρ_i denote porosity, lithology and density of the n-th out of total N minerals. Likewise, S_m and ρ_m are fluid saturation and fluid density for the m-th fluid type out of total M fluids.

The acoustic impedances for compressional (AI_p) and shear (AI_s) waves are given by

$$AI_p = V_p \rho, \tag{2.7a}$$

$$AI_s = V_s \rho. \tag{2.7b}$$

The Poisson's ratio ν describes the ratio of the transverse to the axial strain in a rock under uniaxial stress conditions, and is for isotropic rocks related to the V_p/V_s-ratio via

$$\nu = \frac{0.5(\frac{V_p}{V_s})^2 - 1}{(\frac{V_p}{V_s})^2 - 1}. \tag{2.8}$$

Seismic waves propagating through elastic rocks in a given direction depends on the stiffness tensor $\mathbf{C}$, which in case of isotropic rocks are functions of two elasticity parameters, e.g. K and μ. Rocks with a random geometrical distribution of constituents, generally behave elastically and seismically isotropic (Babuska and Cara 1991). However, rocks with a layering or a preferred alignment of grains or cracks at a scale much smaller than the seismic wavelength will be elastically anisotropic (Thomsen 2002). The simplest form of anisotropy is called transverse isotropy and is defined by five independent constants in the stiffness tensor:

$$\mathbf{C} = \begin{pmatrix} c_{11} & c_{12} & c_{13} & 0 & 0 & 0 \\ c_{12} & c_{11} & c_{13} & 0 & 0 & 0 \\ c_{13} & c_{13} & c_{33} & 0 & 0 & 0 \\ 0 & 0 & 0 & c_{44} & 0 & 0 \\ 0 & 0 & 0 & 0 & c_{44} & 0 \\ 0 & 0 & 0 & 0 & 0 & c_{66} \end{pmatrix}, \tag{2.9}$$

where $c_{66} = (c_{11} - c_{12})/2$. For finely layered rocks, the stiffness constants in equation 2.9 can be expressed by the Backus (1962) averages as

$$\begin{aligned} \bar{c}_{11} &= \langle c_{11} - c_{13}^2 c_{33}^{-1} \rangle + \langle c_{33}^{-1} \rangle^{-1} \langle c_{33}^{-1} c_{13} \rangle^2, \\ \bar{c}_{12} &= \langle c_{12} - c_{13}^2 c_{33}^{-1} \rangle + \langle c_{33}^{-1} \rangle^{-1} \langle c_{33}^{-1} c_{13} \rangle^2, \\ \bar{c}_{33} &= \langle c_{33}^{-1} \rangle^{-1}, \\ \bar{c}_{13} &= \langle c_{33}^{-1} \rangle^{-1} \langle c_{33}^{-1} c_{13} \rangle, \\ \bar{c}_{44} &= \langle c_{44}^{-1} \rangle^{-1}, \\ \bar{c}_{66} &= \langle c_{66} \rangle, \end{aligned} \tag{2.10}$$

where the brackets $\langle \cdot \rangle$ imply a weighted average of the volumetric proportions of the various layers. Five corresponding seismic wave velocities can be defined for various direction of propagation through the layered rock. The fastest and slowest P- and S-wave velocities travel parallel (90°) and perpendicular (0°) to the layering, respectively, and can be expressed by

$$\begin{aligned} V_P(0°) &= \sqrt{\frac{\bar{c}_{33}}{\rho}}, & V_S(0°) &= \sqrt{\frac{\bar{c}_{44}}{\rho}}, \\ V_P(90°) &= \sqrt{\frac{\bar{c}_{11}}{\rho}}, & V_S(90°) &= \sqrt{\frac{\bar{c}_{66}}{\rho}}. \end{aligned} \tag{2.11}$$

Along these directions, phase and group velocities are equivalent.

2.4 Seismic data

The seismic reflection method is the most used remote sensing tool for hydrocarbon exploration and reservoir characterization (Pendrel 2001; Løseth et al. 2009). Seismic observations are measures of traveltime, amplitude, frequency and attenuation of seismic waves propagating through the subsurface and reflected at interfaces between layers of different impedances. Hence, the actual hydrocarbons and reservoir quality are not directly measured, but the impedance contrasts of the subsurface are outlined in terms of amplitude variations. However, it is possible to make predictions of pore fluids and reservoir quality from deriving effective rock physics properties from seismic observables, such as acoustic impedances, seismic velocities and density. This oper-

ation is referred to as seismic inversion (see Figure 2.1), where synthetic and real seismic data is matched (Walden and White 1984; Virieux and Operto 2009; Fichtner 2010). The synthetic data is obtained by using e.g. ray tracing, finite-difference or finite element methods (Robertsson et al. 2007). Also, well data and geological interpretations can be used to guide towards appropriate velocity models (Kolbjørnsen et al. 2016). The synthetic seismic data is then evaluated with respect to how well it fits the real data. In case of a mismatch, the velocity model is accordingly updated until the mismatch becomes sufficiently small. Hence, a more robust velocity model believed to represent the actual subsurface is systematically approached. Figure 2.4 illustrates Norwegian Sea seismic data and well logs used to derive acoustic impedance, where we can see strong amplitudes correspond to high impedance contrasts.

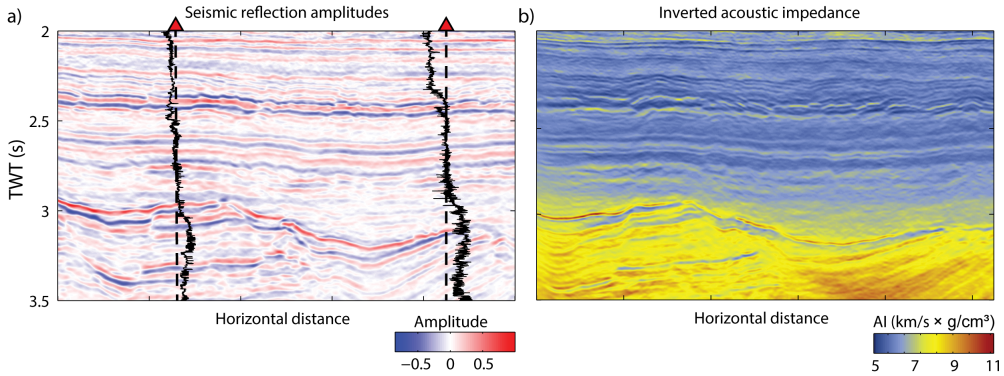

Figure 2.4: (a) Seismic reflection amplitudes and two intersecting acoustic well logs from the Norwegian Sea. (b) The corresponding P-wave impedance (AI) inverted from the seismic reflection amplitudes.

There are several different approaches to seismic inversion including; *i)* deterministic versus probabilistic and *ii)* relative versus absolute (Avseth et al. 2016). Whereas deterministic approaches gives a single solution of a velocity model, the outputs of probabilistic approaches are several possible velocity models and their associated likelihoods through a statistical framework (Cooke and Cant 2010). As such, the various approaches handle the inherent uncertainties of the inverse problem differently, where some are more sophisticated than others (Ball et al. 2016). A further review and discussion of seismic inversion can be found, for instance, in Virieux and Operto (2009), Cooke and Cant (2010), and Fichtner (2010).

2.5 Rock physics modeling

Rock physics modeling addresses a direct link between the reservoir properties (e.g. porosity, lithology and fluids saturation) and the effective rock physics properties (e.g. compressional and shear impedances and velocities) by a set of equations (Grana 2014). The geological characteristics of rocks change continuously from time of deposition through burial via mechanical and

chemical processes. Hence, a library of rock physics models is developed to be applied for various rock types (Mavko et al. 2009; Avseth et al. 2010). In the following, a brief presentation is given of some of the most commonly used rock physics models, that are also used in this study.

Bounds are the simplest types of rock physics models that are based on knowing porosity, constituent properties and respective volume fractions. Despite their simple forms, they are very robust and avoid using complicated idealizations and approximations of the rocks (Avseth et al. 2005). The absolute lower and upper bounds for any isotropic or anisotropic rock can be approximated with the Reuss (Reuss 1929) and Voigt (Voigt 1928) models, respectively. For N constituents they are given by

$$M_R = \left(\sum_{n=1}^{N} \frac{V_n}{M_n} \right)^{-1}, \tag{2.12a}$$

$$M_V = \sum_{n=1}^{N} V_n M_n, \tag{2.12b}$$

where M_R and M_V are the effective elastic moduli (e.g. bulk or shear modulus) of Reuss and Voigt, respectively, and V_n and M_n are the volume fraction and elastic moduli of the n-th constituent, respectively. A physical interpretation of the Reuss model is when stress is applied normally to sequential layers of soft and stiff materials causing equivalent stresses in all layers, while applying stress parallel to the layering gives equivalent strains which describes the Voigt model. Furthermore, the mean of the Reuss and Voigt bounds is given by the Hill average (Hill 1963):

$$M_H = \frac{M_R + M_V}{2}. \tag{2.13}$$

More sophisticated bounding models are introduced by the lower and upper Hashin-Shtrikman bounds (Hashin and Shtrikman 1963). A physical interpretation of the lower bound for a two phase composition is a spherical material with a stiff core and an outer soft shell. The upper bound can be visualized in the same manner when exchanging the stiff and soft constituents. For a two phase composition, the corresponding effective bulk modulus K_{HS} and shear modulus μ_{HS} are given by

$$K_{HS} = K_1 + \frac{V_2}{(K_2 - K_1)^{-1} + V_1 \left(K_1 + \frac{4}{3}\mu_1\right)^{-1}}, \tag{2.14a}$$

$$\mu_{HS} = \mu_1 + \frac{V_2}{(\mu_2 - \mu_1)^{-1} + 2V_1 (K_1 + 2\mu_1) \left[5\mu_1(K_1 + \frac{4}{3}\mu_1)\right]^{-1}}, \tag{2.14b}$$

where V, K and μ are the volume fractions, bulk and shear moduli, respectively, of the two components with indices 1 and 2. The upper and lower bounds are calculated by interchanging which material is termed 1 and which is termed 2. The upper bound is calculated when the

stiffest material is termed 1 and the lower bound when the softest material is termed 1. These equations assume that the material with the highest bulk modulus also has the highest shear modulus, which is not always the case, e.g. for a mixture of calcite ($K = 71$ GPa, $\mu = 30$ GPa) and quartz ($K = 37$ GPa, $\mu = 45$ GPa). A more general form of these bounds compensate for this and is known as the Hashin-Shtrikman-Walpole bounds (HSW), also referred to as the modified Hashin-Shtrikman bounds, and can be written as (Walpole 1966a, 1966b)

$$K_{HSW} = K_1 + \frac{V_2}{(K_2 - K_1)^{-1} + V_1 \left(K_1 + \frac{4}{3}\mu_m\right)^{-1}}, \tag{2.15a}$$

$$\mu_{HSW} = \mu_1 + \frac{V_2}{(\mu_2 - \mu_1)^{-1} + V_1 \left[\mu_1 + \frac{\mu_m}{6}\left(\frac{9K_m + 8\mu_m}{K_m + 2\mu_m}\right)\right]^{-1}}, \tag{2.15b}$$

where the indices 1 and 2 again refer to the properties of the two constituents. The upper bounds are calculated when K_m and μ_m are the maximum bulk and shear moduli of the two constituents, and, vice versa, when they are the minimum bulk and shear moduli, the lower bounds are calculated.

More advanced and theoretical models allow to integrate details about the structure of the rock, such as grain and pore geometry, distribution of the various constituents, along with cementation and pressure conditions. For instance, according to the Hertz-Mindlin contact theory (Mindlin 1949), an idealized package of spherical grains with maximum friction can represent unconsolidated sediments with effective elastic moduli

$$K_{HM} = \left(\frac{n^2 (1 - \phi_0)^2 \mu_s^2}{18\pi^2 (1 - \nu_s)^2} P\right)^{\frac{1}{3}}, \tag{2.16a}$$

$$\mu_{HM} = \frac{5 - 4\nu_s}{5(2 - \nu_s)} \left(\frac{3n^2 (1 - \phi_0)^2 \mu_s^2}{2\pi^2 (1 - \nu_s)^2} P\right)^{\frac{1}{3}}, \tag{2.16b}$$

where K_{HM} and μ_{HM} are the dry-rock bulk and shear moduli, respectively, at depositional porosity ϕ_0; P is the effective pressure; μ_s and ν_s are the shear modulus and Poisson's ratio of the grains; and n is the coordination number which is the average number of contact points that each grain has with surrounding grains. Among others, Murphy (1982) studied how n vary with ϕ in a package of spheres, and can be approximated by:

$$n = 27 - 44\phi + 22\phi^2. \tag{2.17}$$

However, uncertainties arise when trying to distinguish between actual grain contacts and near-grain contacts, which subsequently can lead to erroneous estimations of elastic properties which are completely determined by the load-bearing grain contacts only (Mavko et al. 2009).

As unconsolidated sediments are buried, cementation processes are initiated when the temperature reach 70°C. If cement precipitates at the load-bearing grain contacts, the elastic moduli can be estimated by (Dvorkin and Nur 1996)

$$K_{CCT} = \frac{1}{6} n \left(1 - \phi_0\right) M_c \hat{S}_n, \tag{2.18a}$$

$$\mu_{CCT} = \frac{3}{5} K_{CCT} + \frac{3n \left(1 - \phi_0\right)}{20} \mu_c \hat{S}_\tau, \tag{2.18b}$$

where M_c[1] and μ_c are compressional and shear modulus of the cementing material, respectively. The $\hat{S}_n$ and $\hat{S}_\tau$ parameters are related to the normal and shear contact stiffness, respectively, and are estimated by (Dvorkin and Nur 1996):

$$\begin{aligned}
&\hat{S}_n = A_n b^2 + B_n b + C_n, && \hat{S}_\tau = A_\tau b^2 + B_\tau b + C_\tau, \\
&A_n = -0.024153 \Lambda_n^{-1.3646}, && A_\tau = -10^{-2} \left(2.26\nu^2 + 2.07\nu + 2.3\right) \Lambda_\tau^{0.079\nu^2 + 0.1754\nu - 1.342}, \\
&B_n = 0.20405 \Lambda_n^{-0.89008}, && B_\tau = \left(0.0573\nu^2 + 0.0937\nu + 0.202\right) \Lambda_\tau^{0.0274\nu^2 + 0.0529\nu - 0.8765}, \\
&C_n = 0.00024649 \Lambda_n^{-1.9864}, && C_\tau = 10^{-4} \left(9.654\nu^2 + 4.945\nu + 3.1\right) \Lambda_\tau^{0.01867\nu^2 + 0.4011\nu - 1.8186}, \\
&\Lambda_n = \frac{2\mu_c}{\pi\mu} \frac{(1-\nu)(1-\nu_c)}{(1-2\nu_c)}, && \Lambda_\tau = \frac{\mu_c}{\pi\mu}, \qquad b = \frac{a}{R},
\end{aligned}$$

where μ and ν are the shear modulus and Poisson's ratio of the grains, respectively; μ_c and ν_c are the shear modulus and the Poisson's ratio of the cement, respectively; a and R are the radius of grains with and without an outer shell of cement, respectively. The b parameter can be related to the current porosity ϕ in a cemented sand via certain cement schemes. For instance, if all the cement is concentrated at grain contacts, we get (Dvorkin and Nur 1996)

$$b = 2 \left(\frac{\phi_0 - \phi}{3n(1 - \phi_0)} \right)^{\frac{1}{4}}, \tag{2.19}$$

whereas if the cement is distributed in uniform layers around the grains, we get (Dvorkin and Nur 1996)

$$b = \left(\frac{2(\phi_0 - \phi)}{3(1 - \phi_0)} \right)^{\frac{1}{2}}. \tag{2.20}$$

At the stage when cementation initiates within unconsolidated sediments, the cement can concentrate in distributed patches. Hence, some grains are gradually cemented whereas others are still uncemented such that the rock becomes partly pressure insensitive. Avseth et al. (2012) present a patchy cementation model for such rocks based on mixing the Hertz-Mindlin model

[1] Compressional modulus $M_c = K_c + \frac{4}{3}\mu_c$.

and contact cement model using the Hashin-Shtrikman-Walpole bounds. That means we use equations 2.16 and 2.18 to calculate the effective elastic moduli of uncemented and cemented sediments, respectively, and then insert these into equations 2.15, where the upper and lower Hashin-Sthrikman-Walpole bounds represent various patchy cement schemes. Then, we use the lower Hashin-Shtrikman-Walpole bound to model porosity-sorting effects from the patchy cement end-member to the mineral point at zero porosity.

For more consolidated rocks, a set of models referred to as inclusion models are more relevant. One may, for instance, use the differential effective medium (DEM) model (Berryman 1992), where the effective elastic moduli for a two-phase composite, consisting of a solid mineral with elastic moduli K_s and μ_s with porosity ϕ and pore fluid bulk modulus K_f, can be calculated from the differential equations

$$(1-\phi)\,\frac{d}{d\phi}\left[K_{DEM}(\phi)\right] = \left[K_f - K_{DEM}(\phi)\right] P_2^*(\phi), \tag{2.21a}$$

$$(1-\phi)\,\frac{d}{d\phi}\left[\mu_{DEM}(\phi)\right] = -\mu_{DEM}(\phi) Q_2^*(\phi), \tag{2.21b}$$

where $K_{DEM}(\phi)$ and $\mu_{DEM}(\phi)$ are the effective bulk and shear moduli, respectively, and starting from initial conditions $K_{DEM}(\phi=0) = K_s$ and $\mu_{DEM}(\phi=0) = \mu_s$. P^* and Q^* are geometrical factors associated with the aspect ratio

$$\alpha = \frac{a}{b}, \tag{2.22}$$

where a and b are the minor and major pore axes, respectively.

When a certain fluid or a mixture of various fluids occupy the pore space, pore fluid effects are usually modeled by the Gassmann model (Gassmann 1951). This fluid substitution formula works under the assumptions of an isotropic rock with connected pores that are fully fluid saturated. The effective bulk modulus K_{sat} and shear modulus μ_{sat} can then be calculated by

$$K_{sat} = K_d + \frac{(1-\frac{K_d}{K_s})^2}{\frac{\phi}{K_f} + \frac{1-\phi}{K_s} - \frac{K_d}{K_s^2}}, \tag{2.23a}$$

$$\mu_{sat} = \mu_d, \tag{2.23b}$$

where indices d, s and f denotes dry, solid and fluid, respectively, and ϕ is the porosity. The dry rock properties K_d and μ_d can be calculated from some rock physics model, whereas K_s is the mineral bulk modulus. For a mixture of various fluids, an effective fluid bulk modulus K_f can be estimated using an appropriate mixing law. For a homogeneous fluid mixture, the Reuss bound 2.12a can be used to calculate the effective fluid bulk modulus (Wood 1955). If fluids

are distributed as patches within the pore space, the effective bulk and shear moduli can be calculated using Gassmann's equations for each full fluid saturations, i.e. at $S = 0$ and $S = 1$. Then, the Hill average 2.13 can be used to calculate the effective bulk and shear moduli for varying patchy saturation for the patchy saturated rock. Alternatively, the effective fluid bulk modulus for patchy saturations can be approximated by mixing the various fluids by the Voigt bound 2.12b. In tight cemented sediments, the various fluid mixing models produce similar results, whereas in more unconsolidated sediments, they can differ significantly. Furthermore, for rocks violating the Gassmann assumptions, such as shales with isolated pores, alternative fluid substitution approaches can be used, e.g. the DEM model.

2.6 Methods for seismic interpretation and analysis

Seismic data combined with geological information and well data form the basis for seismic interpretation and analysis. The key challenge is to relate seismic amplitudes to the regional geology and reservoir quality (Avseth et al. 2005; Doyen 2007; Dvorkin et al. 2014). The geophysical toolbox contains many different methods used in hydrocarbon exploration, reservoir characterization, well positioning, and production monitoring. Proper data integration and including geological information opens up for more sophisticated methods to quantify reservoir properties and reduce misinterpretation risks. Below is a brief review of some methods for seismic interpretation and analysis used in this research; for more details see, for instance, Avseth et al. (2005).

2.6.1 Conventional seismic interpretation

Conventional seismic interpretation aims to identify geological structures and stratigraphy from tracking seismic reflection events. Figure 2.5 shows an example where full-stack seismic reflection events are interpreted in terms of layer boundaries and faults in a 2D section.

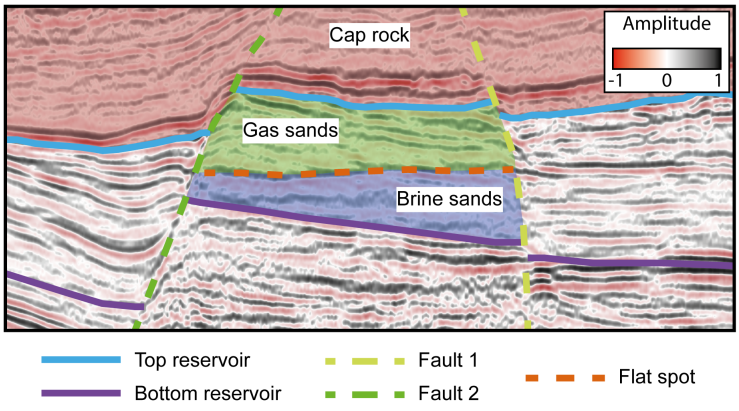

Figure 2.5: Seismic interpretation of a 2D section through a North Sea gas field.

Notice, for instance, the presence of a horizontal flat spot crossing the dipping layers, which can be interpreted as a direct indicator of a hydrocarbon-water contact exhibiting a hard seismic event, i.e. an increase in acoustic impedance and V_p/V_s-ratio. Seismic interpretation can aid in revealing sedimentological and burial history, e.g. the two interpreted fault lines may represent a structural trap of rotational blocks where hydrocarbons have migrated into porous sands located under non-permeable shales. 3D seismic data provide horizons which can be visualized as surface maps indicating structural traps for hydrocarbon accumulation and which subsequently can be used to calculate reservoir volumes. Figure 2.6 shows such a surface map where structural highs represents a top reservoir in a Norwegian Sea oil field.

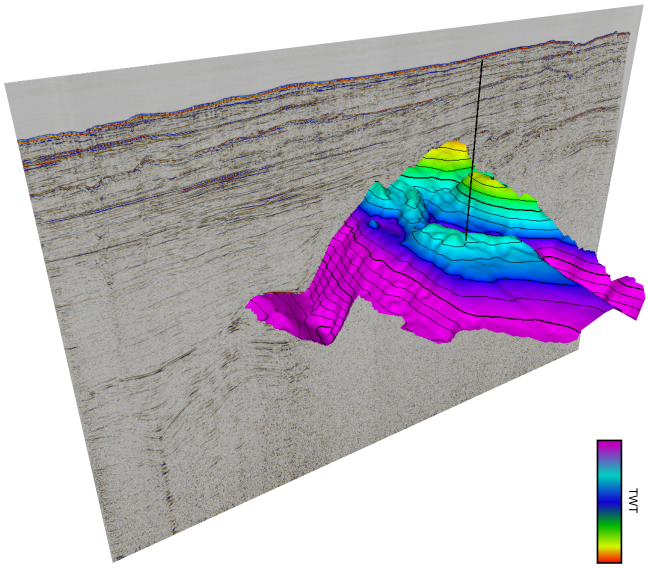

Figure 2.6: Surface mapping based on Norwegian Sea 3D seismic data. TWT, two-way time.

2.6.2 AVO analysis

The interpretation techniques described above are typically carried out on partly or fully stacked seismic data, e.g. near, mid, far or full stacks. Pre-stack gathers reveal variations in reflection amplitudes with offset. This is referred to as Amplitude-Versus-Offset (AVO) analysis and can be used to extract acoustic impedance and V_p/V_s-ratios of the boundary surfaces defining the reflectors. The reflectivity coefficient versus angle of incidence is given by the Zoeppritz equations (Wang 1999). For practical use, approximations to the Zoeppritz equations are often used (e.g. Aki and Richards 1980; Shuey 1985; Smith and Gidlow 1987) with the assumptions of small contrasts in impedances across boundaries, small incidence angles, plane-wave propagation, plane boundaries and isotropic rocks (Mavko et al. 2009). A simplified two-term expression for the P-wave reflection coefficient versus angle of incidence is given by (Wiggins et al. 1983)

$$R_{pp}(\theta) \approx \frac{1}{2}\left(\frac{\Delta V_p}{\bar{V}_p} + \frac{\Delta \rho}{\bar{\rho}}\right) + \left[\frac{1}{2}\left(\frac{\Delta V_p}{\bar{V}_p} + \frac{\Delta \rho}{\bar{\rho}}\right) - \left(\frac{\Delta V_s}{\bar{V}_s} + \frac{\Delta \rho}{\bar{\rho}}\right)\right] \sin^2(\theta), \tag{2.24}$$

assuming $\bar{V}_p/\bar{V}_s = 2$, and where θ is the angle of incidence, and $\Delta V_p = V_{p_2} - V_{p_1}$, $\bar{V}_p = 0.5\,(V_{p_1} + V_{p_2})$ for layers 1 (top) and 2 (bottom), and is equivalent for the S-wave velocity and density. Figure 2.7 illustrates the P-wave reflection coefficient as function of $\sin^2(\theta)$ for $0° \leq \theta \leq 30°$ (equation 2.24) for a boundary between a cap rock (top layer) and gas sandstone reservoir (bottom layer). This linear relationship can be described by only two parameters; the intercept R_0 and gradient G, which are directly related to the P-impedance and S-impedance, respectively, which in turn are sensitive to porosity, lithology and fluid variations. Hence, AVO analysis is often used to predict pore fluids and reservoir quality, given that the cap rock properties do not vary laterally.

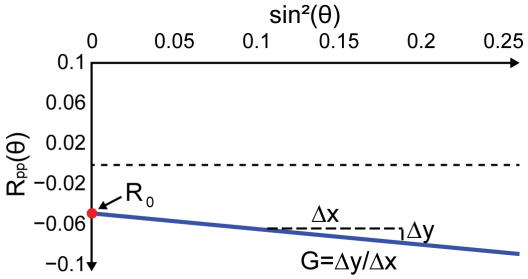

Figure 2.7: P-wave reflection coefficient versus $\sin^2(\theta)$ of incidence for a boundary between a cap rock (top) and gas reservoir rock (bottom).

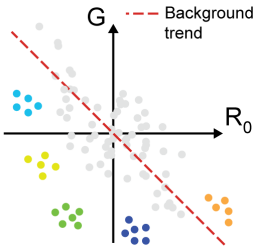

Figure 2.8: Cross-plot of intercept R_0 and gradient G data along a background trend (grey dots) and deviating data (colored dots).

By cross-plotting intercept R_0 versus gradient G data, various classification schemes (e.g. Rutherford and Williams 1989) can be used to study how various lithologies and fluids are located in such cross-plots. Typically, as illustrated in Figure 2.8, the majority of the data will follow a background trend of decreasing G with increasing R_0, which normally is associated with brine-saturated sands interbedded with shales. Hydrocarbon reservoirs may be captured from data points deviating from the background trend (Castagna and Swan 1997; Castagna et al. 1998). Hence, a so-called fluid factor can be defined from the perpendicular distance from the background trend (Smith and Gidlow 1987). Figure 2.9a shows such a fluid factor surface of a top reservoir where warm colors indicate possible oil or gas sands, i.e. data plotting to the lower left in the corresponding AVO cross-plot as illustrated in Figure 2.9b. Some distinctive brightening on structural highs conforms nicely to map contours that may imply an alignment of the hydrocarbon-water contact along with geological structures. Fluid factor maps are useful to get a first impression of the AVO data in terms of prospectivity.

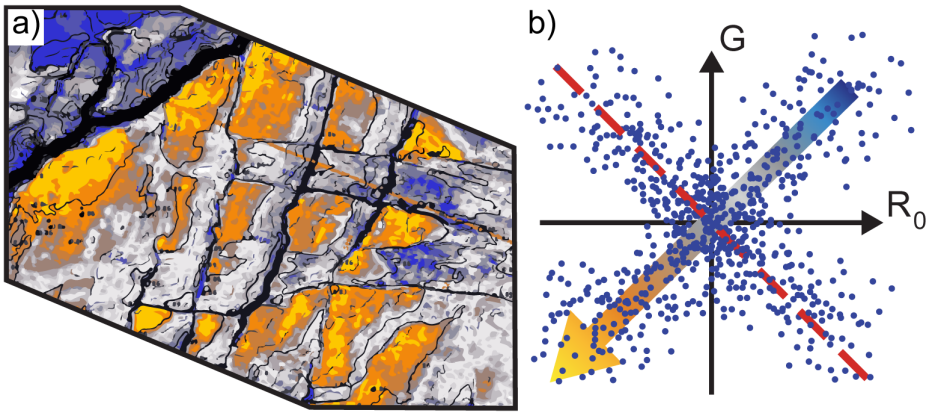

Figure 2.9: (a) Fluid factor surface of a top Barents Sea reservoir with elevation contours superimposed, (b) the corresponding AVO cross-plot where perpendicular distance to the background trend is revealed by the colored arrow.

2.6.3 Rock physics templates

As more well data becomes available in an area, more robust model-based seismic inversion data can be derived (Cooke and Cant 2010) and subsequently combined with rock physics modeling to better obtain quantitative interpretations (Bosch et al. 2010; Grana and Rossa 2010; Avseth et al. 2016). An accessible approach, as illustrated earlier in Figure 2.2, is using rock physics template (RPT) analysis (Ødegaard and Avseth 2004) where a rock physics model is projected on top of a cross-plot of acoustic impedance and V_p/V_s data. Figure 2.10 shows a rock physics template where seismic inversion data from a fairly clean, gas saturated Norwegian Sea sandstone with high porosities around 30-35 % are superimposed.

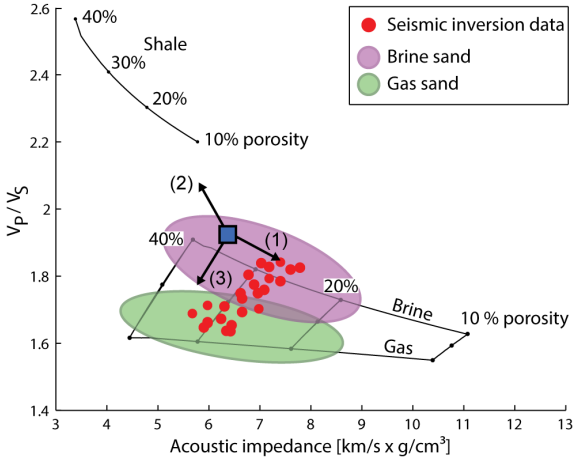

Figure 2.10: Rock physics template analysis.

Also, the blue square illustrates conceptual trends for (1) decreasing porosity, (2) increasing shaliness, and (3) increasing gas saturation for a high-porous brine sandstone (Avseth et al. 2005). Here, the patchy cementation model is used to calculate the dry rock moduli and the Gassmann model is used for fluid substitution.

2.6.4 Inverse rock phyiscs modeling

A more robust method compared to the RPT is inverse rock physics modeling (IRPM) (Johansen et al. 2004, 2013) which emphasize on dealing with the non-uniqueness of the problem. It consists of a two-step procedure:

1. *Forward rock physics modeling*: Calculate rock physics constraints as function of reservoir properties for various effective rock physics properties, e.g. seismic velocities, elastic moduli and acoustic impedances.

2. *Inverse rock physics modeling*: Perform an exhaustive search in the forward modeled constraints for a match with geophysical data, e.g. acoustic impedance and V_p/V_s-ratio from seismic inversion or well log data.

Figure 2.11a illustrates forward modeled constraints from step 1 represented by the bulk and shear moduli for a partly consolidated rock as function of porosity ϕ, lithology C and fluid sat-

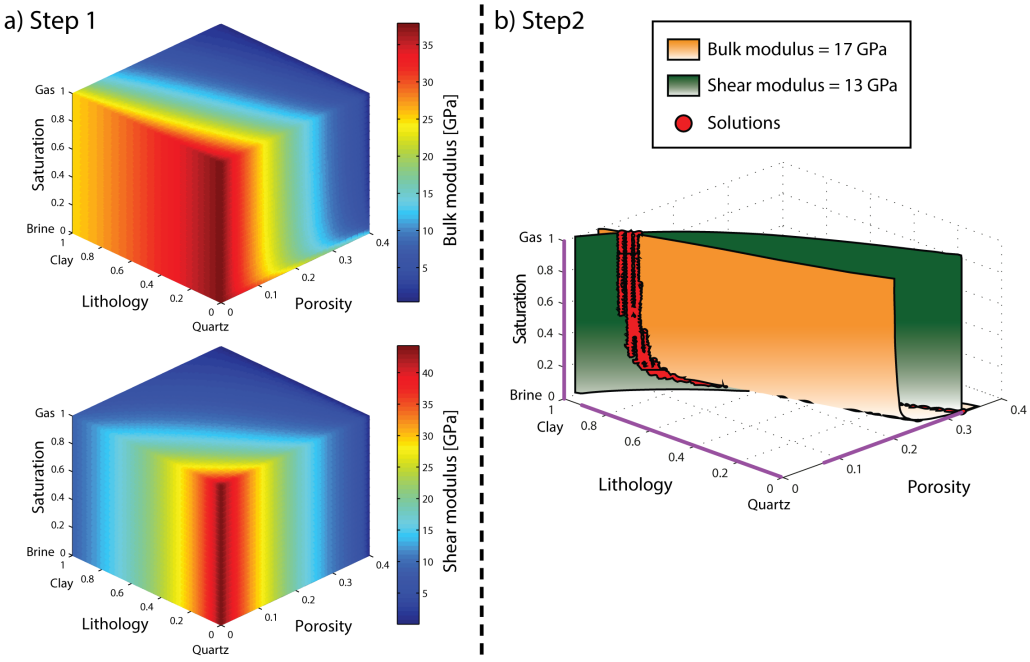

Figure 2.11: The two-step inverse rock physics modeling approach.

uration S (PLF). In step 2, geophysical data provides some particular value, e.g. 17 GPa for the bulk modulus, which corresponds to a so-called isosurface in the bulk modulus constraint cube, consisting of numerous possible PLF solutions (see Figure 2.11b). By combining isosurfaces for correlated geophysical data, e.g. combining the given bulk modulus with a shear modulus of 13 GPa, the solutions are constrained to where the two surfaces intersect; represented by the red dots. Projecting the solution ranges onto the PLF axes (purple intervals), illustrates the issue with non-unique solutions. This is a challenge associated with the specified preconditions of the inverse problem, and not a consequence of the IRPM method itself. The extent of the non-uniqueness will typically vary with the applied rock physics model, choice of data parameters and input values.

The reliability of PLF solutions can further be evaluated based on addressing uncertainties associated with data, e.g. limited signal frequency and noise, and model, e.g. shortcomings in the theoretical models and poor model calibration. For example, model parameters are not assigned specific values, but probability density functions (PDF). A Monte Carlo simulation (Avseth et al. 2005; Doyen 2007; Mavko et al. 2009) is then performed to generate a set of forward modeled constraints. Using modeled density ρ as an example, we do not only model one particular density value, but a range of values for one combination of PLF parameters. For simplicity, we approximate them to have a normal distribution. We can then define a PDF for the density $P(\rho)$ based on the mean density $\bar{\rho}$ and a standard deviation ρ_{std} of this normal distribution (see Figure 2.12).

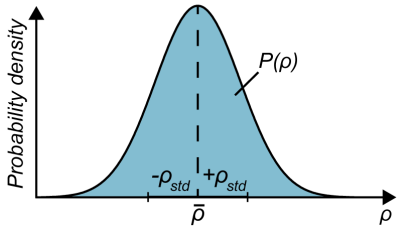

Figure 2.12: A normal PDF for density defined by mean density and standard deviation.

Similarly, the input density data is also not provided as specific values, but as a range of values $\rho_0 \pm \Delta\rho_0$. A likelihood can then be estimated by integrating the normal distribution for the modeled values within this range. Figure 2.13 shows a conceptual illustration of the estimation of model likelihoods. The various identified solutions are plotted in Figure 2.13a color coded by estimated likelihood. The model PDF for one of these solutions are plotted in Figure 2.13b, where the likelihood is highlighted as the integral of the PDF within the specified ranges. Because this likelihood describes how well the data matches the model, we refer to this as the model likelihood. It can be approximated by the Riemann sum

$$P \approx \sum_{i=1}^{N} P(\rho_i)(\rho_i - \rho_{i-1}), \quad -\Delta\rho_0 \leq \rho_i \leq +\Delta\rho_0. \tag{2.25}$$

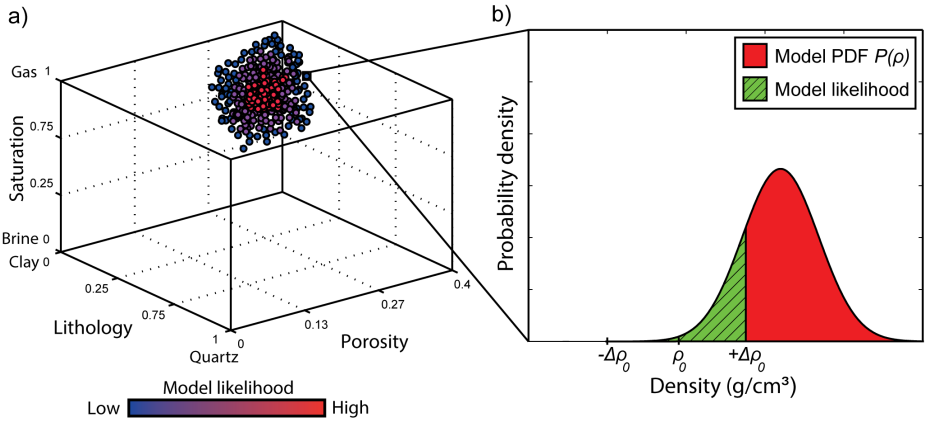

Figure 2.13: (a) All identified solutions and associated model likelihoods estimated from a set of various data parameters, (b) estimating the model likelihood from the density parameter for a particular solution.

If we have knowledge about anticipated reservoir properties, they can be specified as a-priori probabilities, and by using Bayes formula, we can estimate the posterior probability for a particular PLF solution (e.g. Bachrach 2006; Grana and Rossa 2010; Kolbjørnsen et al. 2016). Continuing the example with the density ρ_0 and assuming a rock physics model M_0, the posterior probability $P(\phi, C, S|M_0, \rho_0)$ can be written as

$$P(\phi, C, S|M_0, \rho_0) \propto P(\rho_0|M_0, \phi, C, S)P(\phi, C, S), \tag{2.26}$$

where $P(\rho_0|M_0, \phi, C, S)$ is the estimated model likelihood (see equation 2.25), and $P(\phi, C, S)$ is the a-priori probability. Figure 2.14 shows a conceptual illustration of equation 2.26 by con-

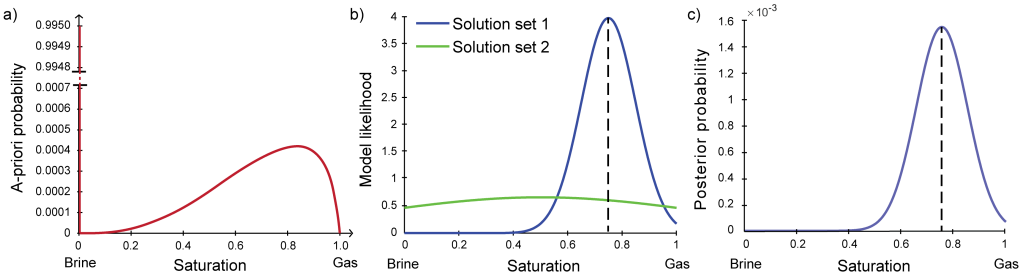

Figure 2.14: A conceptual illustration of (a) a-priori probability, (b) model likelihood, and (c) posterior probability for fluid saturation.

sidering fluid saturation solutions. Figure 2.14a shows a-priori probability for brine saturation defined to be 99.5%, whereas the remaining probability density is given by a mean and standard deviation of 0.7 and 0.19, respectively. The reason behind this a-priori is that the probability for brine is in general very much higher than hydrocarbon saturation. Figure 2.14b illustrates estimated model likelihoods for two different solution sets which are, for convenience, given by normal distributions; solution set 1 is inspired from the identified saturation solutions in Figure 2.13a, with a mean and standard deviation of 0.75 and 0.1, respectively, whereas solution set 2 is given by a value of 0.5 for both mean and standard deviation. Figure 2.14c shows the calculated posterior probability (equation 2.26) from using the model likelihood for solution set 1 and the a-priori probability. Note that the maximum posterior probability has shifted slightly to higher gas saturation compared to the saturation value for maximum model likelihood (vertical stippled lines). However, for solution set 2, the model likelihood gives fairly even predictions for all saturations. Then the a-priori probability will dominate the estimation of the posterior probability; resulting in it being close to zero for anything but pure brine saturation.

A posterior mean $\bar{S}$ can be estimated based on the posterior probabilities (P_i) associated with the various saturation solutions (S_i), given by

$$\bar{S} = \frac{\sum_{i=1}^{N} P_i S_i}{\sum_{i=1}^{N} P_i}, \tag{2.27}$$

where i is an index running over the N possible solutions. If the posterior probability is replaced by the model likelihood for P_i, we instead get an estimate of the weighted mean. Figure 2.15 shows an example comparing weighted and posterior mean, for a vertical section of gas saturation solutions obtained from a Norwegian Sea seismic inversion data set.

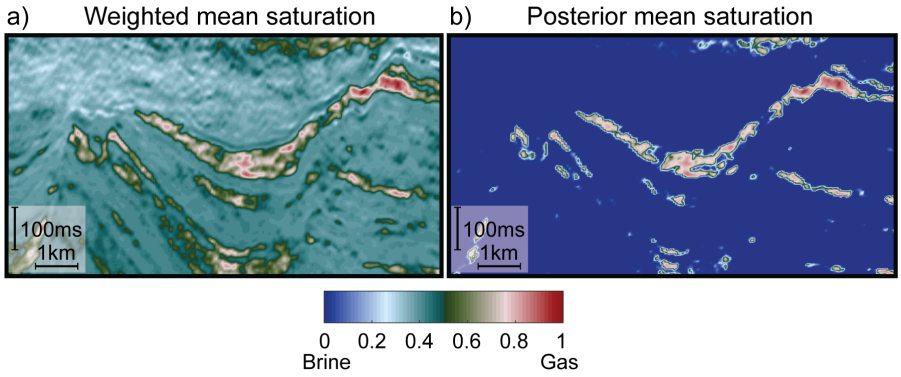

Figure 2.15: IRPM-estimated saturation solutions based on seismic inversion data; represented by a) weighted means from using model likelihood as input, and b) posterior means from using posterior probability as input.

In this example, a 50-50 saturation is predicted in Figure 2.15a where the input data yield no saturation sensitivity for the applied rock physics model. However, using the additional a-priori information in Figure 2.15b dims the gas saturations down to zero, except the areas where a larger model likelihood is estimated for high gas saturations.

Going further, we can also define various facies specified by a range of PLF values. For instance, gas sandstones are expected to have high porosity, low clay content and high gas saturation. We estimate the likelihood of a particular facies and call it the facies identifier (or indicator) P_{facies}, which is given by

$$P_{facies} = P_{F,max} \frac{\sum_{j=1}^{F} P_j}{\sum_{i=1}^{N} P_i}, \tag{2.28}$$

where $P_{F,max}$ is the largest model likelihood for this facies, and P_i and P_j are the model likelihoods, or, the posterior probability if a-priori probability is used, summed over the overall N solutions and total F solutions within the facies. Hence, the facies indicator will be high (close to one) when solutions within are more likely than those outside the facies specifications, as well as there exists at least one solution for that facies with a good match between input and model data. Figure 2.16 shows a conceptual illustration of such a facies indicator for three different saturation solution sets and estimated model likelihood. The green area implies a facies for high gas saturations, whereas the remaining solutions outside the facies are colored blue. Figure 2.16a and b are examples representing high facies indicators due to a relative large model likelihood within the facies as well as a high maximum model likelihood value. Figure 2.16c shows a case where a lower facies indicator is estimated because the model likelihood is more even for all saturations and the maximum model likelihood is lower.

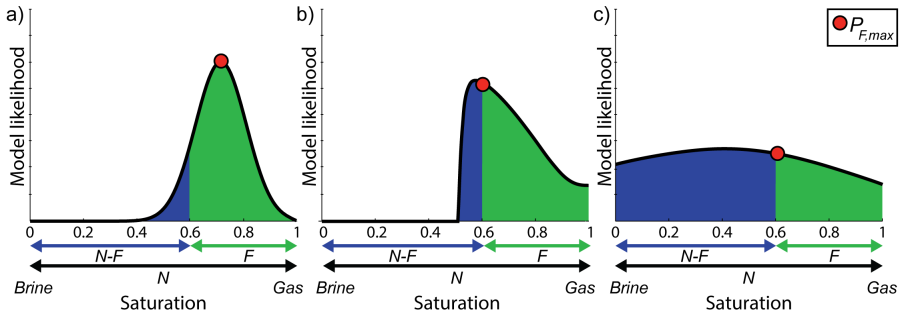

Figure 2.16: Three different saturation solution sets and associated model likelihood within (green) and outside (blue) a specified gas sandstone facies.

The abovementioned IRPM tools make it more flexible to directly analyze solutions consistent with a selection of rock physics models and a set of data. This is different to statistical driven methods dealing with finding the solution with an absolute global minimum of an objective

function. In IRPM a joint exhaustive search for all possible solutions is performed by rock physics relations. Using it to obtain more quantitative interpretations is an iterative process where updated information and observational data can be used to derive more suitable models and constrain solutions. As such, the IRPM is suitable for quantitative interpretation to evaluate the non-uniqueness, correlations and reliability of solutions.

"What we observe is not nature itself, but nature exposed to our method of questioning."

Werner Heisenberg

German theoretical physicist (1901 - 1976)

3

Main scientific contributions

The main scientific contributions of this thesis are given in one conference paper and four research papers that are either published or submitted to peer-reviewed scientific journals. The conference paper contains preliminary results of Paper 1 and was presented at the 75$^{\text{th}}$ EAGE Conference & Exhibition in London 2013. In Paper 1, we demonstrate inverse rock physics modeling (IRPM) based on Norwegian Sea seismic inversion data to predict reservoir quality away from well locations. In Paper 2, we extend the results in Paper 1 and demonstrate source and reservoir rock analysis via a stochastic type of inversion using IRPM applied to some prospective seismic anomalies. In Paper 3, we consider a probabilistic type of inversion using IRPM based on amplitude versus offset (AVO) data and compare the results with using seismic inversion data as considered in Papers 1 and 2. In Paper 4, basin modeling is combined with rock physics to predict seismic velocities of uplifted Triassic sandstones in the Barents Sea and compare these predictions with regional well log data.

Following is a summary of objectives and main findings of each paper. The papers in full forms can be found in the appendix.

3.1 Conference paper: Inverse Rock Physics Modelling on Spatially Varying Seismic Parameters

Kenneth Bredesen, Erling Hugo Jensen and Tor Arne Johansen.

Conference paper, presented at the 75th EAGE Conference & Exhibition, London, 10-13 June, 2013.

The first demonstration of using the inverse rock physics modeling (IRPM) method (Johansen et al. 2004, 2013) for quantitative seismic interpretation was presented in this conference paper. The content shows how we use synthetic seismic parameters for feasibility and performance testing. These preliminary results formed the basis for the continuing research in Papers 1, 2 and 3. Our main findings of this study are:

- We plot 2D sections of mean values and standard deviations to display IRPM predicted reservoir parameters and associated non-uniqueness, respectively.
- A good match between IRPM solutions and the predefined reservoir model was obtained when using the same rock physics models as when generating the synthetic seismic parameters. The corresponding standard deviations were also low.
- When testing single rock physics models on the whole seismic section, solutions were generally found within the facies consistent with the model applied. However, in a couple of instances we also found solutions within wrong facies. This was due to the non-linear effective bulk modulus calculated from the Gassmann fluid substitution model when using a homogeneous fluid mixing model.

3.2 Paper 1: Quantitative seismic interpretation using inverse rock physics modelling

Kenneth Bredesen, Erling Hugo Jensen, Tor Arne Johansen and Per Avseth.

Petroleum Geoscience, 2015, vol. 21, no. 4, 271-284.

Extracting information about reservoir quality from seismic data is a key challenge in exploration, appraisal and production of hydrocarbons. Rock physics modeling offers a solution to this problem consistent with geological information and physical relations. It also allows us to better access quantitative interpretation of seismic data – information that cannot be derived from conventional seismic interpretation.

In this paper we demonstrate inverse rock physics modeling (IRPM) based on real seismic data covering a gas-condensate Norwegian Sea field. A three-step procedure is used comprising (1) seismic inversion, (2) forward- and (3) inverse rock physics modeling, where our focus is on steps 2 and 3. The objective of this study is to predict porosity, clay-to-sand fraction and gas-to-brine fluid saturation along a seismic cross-section where we have well control. The main findings of this study are:

- Petrophysical well logs intersecting the seismic cross-section was used to evaluate a range of rock physics models for two gas sandstone reservoirs in our study area. For this, we used

rock physics templates in an initial screening phase to identify relevant model candidates. Subsequently, IRPM was used to further calibrate and fine-tune input model parameters. We finally selected a patchy cementation model that gave a good match to the petrophysical well logs.

- A nearby blind well was used to test the performance and robustness of our calibrated rock physics model by using IRPM and showed a good match between solutions and petrophysical logs.

- The calibrated rock physics model was used as input to IRPM together with sections of acoustic impedance, P-to-S velocity ratio and density to predict reservoir quality away from well location. Reasonable solutions were obtained at the well bore that followed interpreted reservoir boundaries consistently.

- Some parts of the reservoir units exhibit very low P-to-S velocity ratios that consequently gave no solutions in our forward modeled constraints.

- Solutions obtained using a combination of acoustic impedance and P-to-S velocity ratio was compared to solutions based additionally on density. Neglecting the density parameter gave more consistent solutions of the reservoir properties but also less constrained solutions with higher standard deviations.

- The current methodology use a simplified tolerance factor to address uncertainties that cannot be explicitly related to data or model uncertainties. This require more sophisticated uncertainty handling for more robust reservoir characterizations and risk assessments.

3.3 Paper 2: Seismic reservoir and source-rock analysis using inverse rock-physics modeling: A Norwegian Sea demonstration

Kenneth Bredesen, Erling Hugo Jensen, Tor Arne Johansen and Per Avseth.

The Leading Edge, 2015, vol. 34, no. 11, 1350-1355.

Identifying type of rocks and fluids from seismic amplitude anomalies can be challenging because various rocks can exhibit similar seismic responses. Lithology and fluid predictions based on seismic properties are therefore often associated with uncertainties. The Upper Jurassic stratigraphy on the Norwegian Shelf is an example which comprise organic rich shales with embedded high reservoir quality sandstones. Several recent wells on the Norwegian Shelf missed out on these sandstones and encountered thick intervals of organic rich shales instead. Distinguishing

high porosity clean sandstones and organic rich shales have turned out to be a key challenge in recent hydrocarbon explorations.

In this paper the inverse rock physics modeling (IRPM) from Paper 1 is extended using a stochastic inversion method. This allows us to evaluate the likelihood of solutions for a given rock physics model and input data. Based on this, our objective is to find out whether some intrawell seismic anomalies in an Upper Jurassic prospect in the Norwegian Sea represents organic rich shales or potential reservoir sandstones. The main findings of this study are:

- Two rock physics models were calibrated from using IRPM with regional well log data; one well penetrates a gas sandstone reservoir and another well penetrating an organic rich shale formation.

- The solutions obtained from the rock physics model for the gas sandstone reservoir showed a higher likelihood within the target interval than the corresponding solutions for the organic rich shales.

- The solutions and estimated model likelihoods are evaluated based on a weighted mean and facies indicator.

- The solutions for the gas sandstone reservoir shows promising reservoir quality with high porosities, low clay content and high gas saturations within the target interval.

- Modeling organic rich shales is a fairly new terrain and claims for better understanding of how their seismic properties vary with pore geometry, constituent properties, and organic content and maturation. Also, we have assumed isotropic rocks by only using normal-bedding properties, even though organic rich shales are known for strong anisotropy.

- The well log data penetrating the organic rich shale lacks important petrophysical information, which counteracts an accurate model calibration. Hence, the solutions for the organic rich shale, such as kerogen content predictions, are very uncertain. However, it could still be useful for quick facies screenings and to obtain reliable trends.

3.4 Paper 3: Quantitative interpretation using inverse rock-physics modeling on AVO data

Erling Hugo Jensen, Tor Arne Johansen, Per Avseth and Kenneth Bredesen.

The Leading Edge, 2016, vol. 35, no. 8, 677-683.

In frontier exploration, poor well coverage counteracts deriving robust seismic inversion data often used for quantitative interpretations. However, continuous advancement in computer capacity has driven many geophysicists towards interpretation of pre-stack seismic data; a door opener for fluid and lithology predictions. A pre-stack gather yields access to amplitude versus offset (AVO) data for a given geological boundary, and can vary considerably with different fluid and lithology scenarios.

In this paper, the inverse rock physics modeling (IRPM) method is developed a step further to accept AVO data as input. Also, the stochastic inversion in Paper 2 is combined with Bayes Theorem which yields a probabilistic type of inversion using IRPM. As such, regionally calibrated rock physics models can be used to obtain more quantitative interpretations than possessed by conventional AVO classification schemes. We use a calibrated rock physics model from Paper 2 together with AVO data covering the same Norwegian Sea area. The solutions are compared with the results obtained by seismic inversion data, as considered in Paper 1 and 2. The main findings of this study are:

- AVO intercept and gradient constraint cubes are forward modeled using fixed properties for a cap-rock overlying a reservoir rock modeled by a rock physics model with a range of possible porosity, lithology and fluid saturation combinations.

- From using the Bayes formula based on an estimated model likelihood and a-priori probability, the posterior probability of solutions are calculated and then evaluated by a weighted posterior and facies indicator.

- The reservoir solutions based on AVO data and seismic inversion data as input are very much in agreement, and shows consistency with well log data.

- Using AVO data provides a robust alternative to using more resource demanding and expensive seismic inversion data as input.

- The different solution sets obtained from AVO and seismic inversion data must be interpreted differently because AVO represents elastic contrasts between layers, whereas seismic inversion yields average layer properties.

- The solutions obtained using AVO data implies additional prospectivity in a graben setting, corresponding to that considered in Paper 2. However, the solutions appear more spatially fragmented, implying a probable false-positive.

3.5 Paper 4: Rock physics modelling based on burial history of Barents Sea sandstones

Kenneth Bredesen, Per Avseth, Tor Arne Johansen and Richard Olstad.

Submitted to Petroleum Geoscience, May 2016.

During the last decades, several promising Barents Sea prospects have been drilled in frontier areas with disappointing results. Well log data have several times shown abnormally low acoustic velocities within reservoir sandstones, which does not agree well with conventional rock physics models for these rock types. Present day rock physics and related seismic responses are influenced by ancient geological processes and events. The geological setting and history of the arctic Barents Sea, which has been considerably uplifted the last million years, is known for being highly complex. Hence, a better incorporation of basin history with rock physics can help our understanding of what is causing the abnormal velocity observations.

In this paper, we combine basin modeling and rock physics to predict seismic velocities and match these with well log data of the Kobbe sandstone in the Barents Sea. Two small gas discoveries at the Bjarmeland platform are considered together with an oil-gas discovery in the Hammerfest basin. Time-depth curves are derived from basin modeling which are subsequently used to estimate porosity and quartz cement volume from kinetic equations. These rock texture parameters are then inserted into rock physics models valid for various burial and uplift domains. The overall objective is to demonstrate how rock physics can be combined with basin modeling to better understand how complex geological history may influence seismic properties to infer better prospect evaluations of uplifted reservoirs. The main findings of this study are:

- Seismic velocities were predicted as function of depth and time that gave a reasonable match to well log data.
- Our velocity predictions implies that rock physics models addressing increasing cementation only overpredicts velocities, whereas using a model which additionally honors microcracks match the data better.
- We suspect the modeled microcracks to be related to overburden unloading and subsequent stress relaxation during uplift events.
- A range of uncertainties follows our model approach as a high number of unknown variables are related to assigning parameters to ancient geological conditions. Some of these aspects are included in our modeling, whereas others are simplified, e.g. assuming a constant geothermal gradient and isotropic rocks.

- There are yet open questions to how and at which rate microcracks forms during uplift and how the cement precipitates at grains. Hence, the velocity curves can have a more complex signature than proposed by our predictions.
- In spite of all inherent uncertainties, our velocity predictions can give useful trends to be compared with well log and seismic velocities to support regional interpretation, play fairway assessments and prospect definition.

"If the facts don't fit the theory, change the facts."

Albert Einstein

German physicist & philosopher (1879 - 1955)

4

Conclusions

In this study, geophysical analysis consistent with rock physics are performed for better quantitative interpretation of reservoir properties. Both synthetic and real data from the Norwegian Shelf are used to demonstrate practical applications. The main conclusions are:

- The feasibility and performance of using inverse rock physics modeling based on seismic data was tested and verified by considering a synthetic data set.
- Reservoir property predictions were successfully demonstrated on Norwegian Sea seismic inversion data using inverse rock physics modeling. The predictions were in good agreement with nearby well data.
- A stochastic inverse rock physics modeling approach was used for seismic screening of reservoir and source rocks. Some seismic anomalies in a Norwegian Sea prospect showed that these most likely represent high quality gas saturated reservoir sandstones and not source rocks.
- A probabilistic inverse rock physics modeling approach based on AVO data was used for reservoir property predictions. The predictions were compared with seismic inversion data as input and showed a good agreement.
- Seismic velocities of uplifted sandstones in the Barents Sea are predicted by using appropriate rock physics models conditioned by basin history. Whereas conventional rock physics modeling overpredicts velocities, a better match to regional well log data was achieved when first honoring mechanical and chemical compaction and then including cracks.

"All the business of life is to endeavour to find out what you don't know by what you do..."

Arthur Wellesley

1st Duke of Wellington (1769 - 1852)

5
References

Aki, K., and P.G. Richards. 1980. *Quantitative seismology: theory and methods*. San Francisco.

Avseth, P., and J.M. Carcione. 2015. "Rock-physics analysis of clay-rich source rocks on the Norwegian Shelf". *The Leading Edge* 34:1340–1348. doi:10.1190/tle34111340.1.

Avseth, P., A. Janke, and F. Horn. 2016. "AVO inversion in exploration–Key learnings from a Norwegian Sea prospect". *The Leading Edge* 35:405–414. doi:10.1190/tle35050405.1.

Avseth, P., T. Mukerji, and G. Mavko. 2005. *Quantitative Seismic Interpretation*. Cambridge University Press. ISBN: 9780521151351.

Avseth, P., T. Mukerji, G. Mavko, and J. Dvorkin. 2010. "Rock-physics diagnostics of depositional texture, diagenetic alterations, and reservoir heterogeneity in high-porosity siliciclastic sediments and rocks – A review of selected models and suggested work flows". *Geophysics* 75:31–47. doi:10.1190/1.3483770.

Avseth, P., N. Skjei, and G. Mavko. 2012. "Rock physics modelling of stress sensitivity in patchy cemented sandstones". *Paper I009, presented at the 74th EAGE Conference and Exhibition, Copenhagen, 4-7 June*. doi:10.3997/2214-4609.20148295.

Babuska, V., and M. Cara. 1991. *Seismic Anisotropy in the Earth*. Springer. ISBN: 9789401055963.

Bachrach, R. 2006. "Joint estimation of porosity and saturation using stochastic rock-physics modeling". *Geophysics* 71:53–63. doi:10.1190/1.2235991.

Backus, G.E. 1962. "Long-Wave Elastic Anisotropy Produced by Horizontal Layering". *Journal of Geophysical Research* 67:4427–4440. doi:10.1029/JZ067i011p04427.

Ball, V., M. Nasser, and Kolbjørnsen. 2016. "Introduction to this special section: AVO inversion". *The Leading Edge* 35:399–404. doi:10.1190/tle35050399.1.

Berryman, J.G. 1992. "Single scattering approximations for coefficients in Biot equations of poroelasticity". *Journal of the Acoustical Society of America* 91:551–571. doi:10.1121/1.402518.

Bosch, M., T. Mukerji, and E.F. Gonzalez. 2010. "Seismic inversion for reservoir properties combining statistical rock physics and geostatistics: A review". *Geophysics* 75:165–176. doi:10.1190/1.3478209.

Castagna, J.P., and H.W. Swan. 1997. "Principles of AVO crossplotting". *The Leading Edge* 16:337–344. doi:10.1190/1.1437626.

Castagna, J.P., H.W. Swan, and D.J. Foster. 1998. "Framework for AVO gradient and intercept interpretation". *Geophysics* 63:948–956. doi:10.1190/1.1444406.

Cooke, D., and J. Cant. 2010. "Model-based Seismic Inversion: Comparing deterministic and probabilistic approaches". *CSEG Recorder* 35:28–39.

Doyen, P.M. 2007. *Seismic Reservoir Characterization: An Earth Modeling Perspective*. EAGE Publications bv. ISBN: 9789073781771.

Dvorkin, J., M.A. Gutierrez, and D. Grana. 2014. *Seismic Reflections of Rock Properties*. Cambridge University Press. ISBN: 9780521899192.

Dvorkin, J., and A. Nur. 1996. "Elasticity of high-porosity sandstones: Theory for two North Sea data sets". *Geophysics* 61:1363–1370. doi:10.1190/1.1444059.

Fichtner, A. 2010. *Full seismic waveform modelling and inversion*. Springer Science & Business Media. ISBN: 9783642158070.

Gassmann, F. 1951. "Elastic waves through a packing of spheres". *Geophysics* 16:673–685. doi:10.1190/1.1437718.

Grana, D. 2014. "Probabilistic approach to rock physics modeling". *Geophysics* 79:123–143. doi:10.1190/geo2013-0333.1.

Grana, D., and E.D. Rossa. 2010. "Probabilistic petrophysical-properties estimation integrating statistical rock physics with seismic inversion". *Geophysics* 75:21–37. doi:10.1190/1.3386676.

Hashin, Z., and S. Shtrikman. 1963. "A variational approach to the theory of the elastic behaviour of multiphase materials". *Journal of the Mechanics and Physics of Solids* 11:127–140. doi:10.1016/0022-5096(63)90060-7.

Hill, R. 1963. "Elastic properties of reinforced solids: Some theoretical principles". *Journal of the Mechanics and Physics of Solids* 11:357–372. doi:10.1016/0022-5096(63)90036-X.

Johansen, T.A., E.H. Jensen, G. Mavko, and J. Dvorkin. 2013. "Inverse rock physics modeling for reservoir quality prediction". *Geophysics* 78:1–18. doi:10.1190/geo2012-0215.1.

Johansen, T.A., K. Spikes, and J. Dvorkin. 2004. "Strategy for estimation of lithology and reservoir properties from seismic velocities and density". *Paper SEG-2004-1726, presented at the SEG International Exhibition and 74th Annual Meeting, Denver, 10-15 October*. doi:10.1190/1.1845162.

Kolbjørnsen, O., A. Buland, R. Hauge, P. Røe, M. Jullum, R.W. Metcalfe, and Ø. Skjæveland. 2016. "Bayesian AVO inversion to rock properties using a local neighborhood in a spatial prior model". *The Leading Edge* 35 (5): 431–436. doi:10.1190/tle35050431.1.

Løseth, H., M. Gading, and L. Wensaas. 2009. "Hydrocarbon leakage interpreted on seismic data". *Marine and Petroleum Geology* 26:1304–1319. doi:10.1016/j.marpetgeo.2008.09.008.

Mavko, G., T. Mukerji, and J. Dvorkin. 2009. *The Rock Physics Handbook*. Cambridge University Press. ISBN: 9780521861366.

Mindlin, R.D. 1949. "Compliance of elastic bodies in contact". *Journal of Applied Mechanics* 16:259–268. doi:10.1007/978-1-4613-8865-4_24.

Murphy, W.F. 1982. *Effects of Microstructure and Pore Fluids on the Acoustic Properties of Granular Sedimentary Materials*. Ph.D. thesis, Stanford University, USA.

Ødegaard, E., and P. Avseth. 2004. "Well log and seismic data analysis using rock physics templates". *First Break* 22:37–43. doi:10.3997/1365-2397.2004017.

Pendrel, J. 2001. "Seismic inversion – The best tool for reservoir characterization". *CSEG Recorder* 26:18–24.

Qin, X., D. Han, and L. Zhao. 2014. "Rock physics modeling of organic-rich shales with different maturity levels". *Expanded Abstracts, presented at the SEG Annual Meeting, Denver*: 2952–2957. doi:10.1190/segam2014-1584.1.

Reuss, A. 1929. "Berechung der Fließgrenze von Mischkristallen auf Grund der Plastizitätsbedingung für Einkristalle". *ZAMM - Journal of Applied Mathematics and Mechanics / Zeitschrift für Angewandte Mathematik und Mechanik* 9:49–58. doi:10.1002/zamm.19290090104.

Robertsson, J.O., B. Bednar, J. Blanch, C. Kostov, and D.J. van Manen. 2007. "Introduction to the supplement on seismic modeling with applications to acquisition, processing, and interpretation". *Geophysics* 72:1–4. doi:10.1190/1.2755959.

Rutherford, S.R., and R.H. Williams. 1989. "Amplitude versus offset variations in gas sands". *Geophysics* 54:680–688. doi:10.1190/1.1442696.

Shuey, R.T. 1985. "A simplification of the Zoeppritz equations". *Geophysics* 50:609–614. doi:10.1190/1.1441936.

Smith, G.C., and P.M. Gidlow. 1987. "Weighted stacking for rock property estimation and detection of gas". *Geophysical Prospecting* 35:993–1014. doi:10.1111/j.1365-2478.1987.tb00856.x.

Thomsen, L. 2002. *Understanding Seismic Anisotropy in Exploration and Exploitation*. Vol. 5. Society of Exploration Geophysicist. ISBN: 9781560801122.

Virieux, J., and S. Operto. 2009. "An overview of full-waveform inversion in exploration geophysics". *Geophysics* 74:1–26. doi:10.1190/1.3238367.

Voigt, W. 1928. *Lehrbuch der Kristallphysik (mit Ausschluss der Kristalloptik)*. 4427–4440. B.G. Teubner J.W. Edwards. ISBN: 9783663158844.

Walden, A.T., and R.E. White. 1984. "On Errors of Fit and Accuracy in Matching Synthetic Seismograms and Seismic Traces". *Geophysical Prospecting* 32:871–891.

Walpole, L.J. 1966a. "On bounds for the overall elastic moduli of inhomogenous systems–I". *Journal of the Mechanics and Physics of Solids* 14:151–162. doi:10.1016/0022-5096(66)90035-4.

— . 1966b. "On bounds for the overall elastic moduli of inhomogenous systems–II". *Journal of the Mechanics and Physics of Solids*. doi:10.1016/0022-5096(66)90025-1.

Wang, Y. 1999. "Approximations to the Zoeppritz equations and their use in AVO analysis". *Geophysics* 64:1920–1927. doi:10.1190/1.1444698.

Wiggins, R., G.S. Kenny, and C.D. McClure. 1983. "A method for determining and displaying the shear-velocity reflectivities of a geologic formation". *European Patent Application* 113944.

Wood, A.B. 1955. *A textbook of sound: being an account of the physics of vibrations with special reference to recent theoretical and technical developments*. G. Bell. doi:10.1063/1.3059819.

"You have enemies? Good. That means you've stood up for something, sometime in your life."

Winston Churchill

British politician (1874 - 1965)